Toward Unified Biomarkers for Focal Epilepsy

Sheng H Wang[1–5], Paul Ferrari[5,6], Gabriele Arnulfo[7], Morgane Marzulli[1,2,8], David Degras[1,2,9], Vladislav Myrov[4], Satu Palva[3,10], Lino Nobili[11,12], Philippe Ciuciu[1, 2†], J Matias Palva[†3,4,10]

[†]These authors contributed equally to this work.

Author affiliations:

1. CEA, NeuroSpin, France.
2. MIND, Inria, Université Paris-Saclay, France.
3. Neuroscience Center, Helsinki Institute of Life Science, University of Helsinki, Finland.
4. Department of Neuroscience and Biomedical Engineering, Aalto University, Finland.
5. Jack H. Miller MEG Center, Helen DeVos Children's Hospital, Corewell Health, USA.
6. Department of Pediatrics and Human Development, Michigan State University, USA.
7. Department of Informatics, Bioengineering, Robotics and System engineering, University of Genoa, Italy.
8. Université Paris Cité, France.
9. Department of Mathematics, University of Massachusetts Boston, USA.
10. School of Psychology and Neuroscience, University of Glasgow, United Kingdom.
11. Child Neuropsychiatry Unit, IRCCS Istituto Giannina Gaslini, member of the European Reference Network EpiCARE, Italy.
12. Department of Neurosciences, Rehabilitation, Ophthalmology, Genetics and Maternal and Children's Sciences, University of Genoa, Italy.

Correspondence to:
Sheng H. Wang
Full address: CEA, Joliot, NeuroSpin, Bât. 145,
Point Courrier 156, 91191
Gif-sur-Yvette cedex, France.
E-mail: sheng.wang@helsinki.fi

Running title: Toward Unified Epilepsy Biomarkers

Keywords: criticality, synchrony, epileptogenic zone, biomarker, latent space, tensor components

Abstract

Surgical resection of the epileptogenic zone (EZ) is the most effective treatment for drug-resistant focal epilepsy. However, 30–80% of patients do not attain long-term seizure freedom post-surgery, indicating that presurgical evaluation often falls short of fully delineating the EZ. Accurate EZ-localization is challenging because each individual EZ is a unique and complex network, often comprising multiple overlapping neuropathologies. This hypothesis is supported by studies showing that combining multiple biomarkers enhances localization accuracy. Nonetheless, combining biomarkers leads to high-dimensional features that risks overfitting classifiers and reduces the interpretability of underlying neuropathology, ultimately limiting clinical applicability.

We asked whether high-dimensional neuronal features could be reduced to a low-dimensional latent space to captures essential characteristics of the epileptogenic network (EpiNet). In this latent space, each sampled brain region is assigned an EpiNet-saliency score along a 0–1 continuum, characterizing the degree of epileptogenic proneness from lowest to highest. Using 10-minute interictal recordings from 7,183 stereo-EEG (SEEG) contacts across 64 focal epilepsy patients, we extracted 260 features of local and network dynamics. Singular value decomposition of these raw features revealed that ten eigenfeatures were sufficient to identify the seizure-zone (SZ) where seizures emerged. These eigenfeatures were used to train two unsupervised classifiers, which converged on a consensus model for assessing EpiNet-saliency using only the first and second eigenfeatures, reducing the dimensionality to 0.77% of the raw feature set. The resulting model was tested on 7–9 hours of sleep-SEEG recording from three patients in an independent cohort and validated with tensor component analysis.

Among the 64 subjects, SZ-classification accuracy correlated with individual position in the eigenfeature space (r^2=0.5), suggesting that variability in EpiNet-saliency contributes to differences in classification performance. The model then successfully captured time-varying EpiNet-saliency in the sleep-SEEG, corroborating clinical assessments and achieving peak classification accuracies of 0.63, 0.85, and 0.94, respectively. Within-subject tensor component analysis validated the spatiotemporal characteristics of model-predicted EpiNet-saliency in the sleep-SEEG.

These results provide compelling evidence supporting our hypothesis of a low-dimensional representation of epileptogenicity, which appears to be independent of brain state or neuropathological origin. This innovative approach enables straightforward interpretation of neuropathology and facilitates the integration of additional biomarkers and study of large cohorts, owing to its minimal computational footprint. These advancements significantly enhance the feasibility of a framework for unified epilepsy biomarkers.

Introduction

Epilepsy affects 1% of the general population, with 30–40% of patients being drug-resistant (DRE)[1]. The most effective treatment for gaining seizure control in focal onset DRE is surgical resection or disconnection of the seizure-causing brain tissue known as the epileptogenic zone (EZ). A growing body of recent research[2–5] suggests rather than a single discrete EZ or seizure focus, multiple overlapping neuropathological substrates form an epileptogenic network (EpiNet) that collectively responsible for generating seizures. The EpiNet can be a combination of structural lesion[6], high frequency oscillations (HFO) zone[7], irritative (spiking) zone[8], and seizure zone[3]. Various biomarkers have been proposed to localize these epileptogenic mechanisms[9,10]. However, surgical outcomes vary significantly, with 30% to 70% patients experiencing seizure recurrence within few months of surgery[11,12], suggesting that accurate EpiNet localization remains a current challenge.

We recently advanced novel epilepsy biomarkers inspired by complex systems theory and the brain criticality hypothesis[13–15]. We proposed that the brain functions optimally when operating in a critical regime between order and disorder[14,16]. Empirical evidence linking aberrant brain criticality to epilepsy includes abnormal power-law scaling[13,17], strong inhibition[18,19], and high bistability in neuronal oscillations[18,20] that suggests a shift towards catastrophic events like that in many complex systems[15,21]. Aberrant local criticality is believed to coexist with a large-scale trend towards supercriticality, characterized by elevated synchrony within and around the EpiNet[14]. Utilizing both local and large-scale biomarkers has yielded more accurate localization compared to individual biomarkers[18], thereby offering support for the multi-component hypothesis for the EZ[3].

However, employing multiple biomarkers to assess dozens of narrow-band oscillations leads to high dimensional (high-D) feature sets, posing a major challenge to advancing automated, data driven localization. Having hundreds or thousands of features requires enormous computational resources and makes results interpretation difficult for physicians. It also risks over-fitting and prevents efficient training of machine learning models. This impedes the addition of novel[22,23] biomarkers or established clinical biomarkers, such as HFO, slow waves, and spikes, thus hindering the efforts to study their functional relationships and to understand why clinical biomarkers often lose specificity in practice[24]. Moreover, the classifiers used earlier has high overhead and may handle thousands of sampled brain regions but would

become impractical for studying larger clinical data. Therefore, we aimed to advance a new framework that would simplify feature interpretation and resolve technical challenges in training models for automated EpiNet-localization.

We hypothesized that, while the large-scale EpiNet is most comprehensively characterized by simultaneously employing multiple local and large-scale biomarkers (Fig. 1A), the essential epileptogenic dynamics should fluctuate slowly in a low-dimensional (low-D) latent state space (Fig. 1B)—like that has been proposed in local epileptogenic bifurcation models[25–28]—with each latent feature corresponds to a distinct set of epileptogenic raw feature pattern interictally observable. Brain regions from the EpiNet, regardless of whether or not they engage in seizures during the recording, should exhibit mid- and high-risk regime corresponding to increased epileptogenic feature saliency (λ) in the latent space, (Fig 1C)[3,18]. This latent space can be approximated by a low-rank eigenfeature space, derived from raw features of interictal, resting-state brain activity[29].

Materials and methods

A model for assessing the EpiNet feature saliency was trained using resting-SEEG from 64 patients (Fig. 1D). The initial 260 raw resting features were reduced to ten eigenfeatures capable of differentiating the seizure zone (SZ) from where seizures activity was identified by physicians. These eigenfeatures were then used to train two unsupervised classifiers to construct the model for identifying the EpiNet contacts—contacts bearing similar epileptogenic characteristics—regardless of their clinical SZ or non-SZ classification by the physicians. To validate the model across domains, it was tested using sleep-SEEG from a separate cohort. Time-resolved raw sleep features were linearly projected into resting-SEEG's eigenfeature space (Fig. 1E). The resulting coefficients served as inputs for the EpiNet-saliency model. The model's assessments were evaluated against clinically identified cortical dysplasia and then validated by tensor component analysis.

Subjects and recording

The training set included 7,183 SEEG contacts from 64 patients (mean ± SD age: 29.7 ± 9.5, 29 females) with focal onset seizures treated at the Niguarda "Ca' Granda" Hospital, Milan, Italy. They underwent SEEG for the first time and had no prior epilepsy surgery. Ten-minute of eyes-closed, resting-state brain activity were recorded with SEEG, ensuring no seizure

activity at least one hour before and after these recordings[30]. On average the subjects had 113±16.2 (±SD) contacts recorded from grey-matter, and the recordings were referenced using the nearest white-matter contact[31]. The test set included three patients from a separate cohort treated at the same institute. Their epilepsy was caused by type-2 focal cortical dysplasia (FCD), confirmed by post-surgical histopathological study. These patients were chosen because FCD represents a prototypical clinical model of sleep-related epilepsy with a well-characterized histopathological substrate[32], and all of them achieved seizure freedom (Engel class 1A) at a minimum of one-year follow-up, validating accurate EZ localization and resection. Structural MRI and post-implant CT data were unavailable, and a bipolar referencing scheme was used for them. All training and test subjects were under anti-seizure medication. The time from the last drug administration to SEEG recording was not controlled, and the drug effects on individual epileptogenic features therefore were not considered. All subjects gave written informed consent for participation in research studies and for publication of results pertaining to their data. This study was approved by the ethical committee (ID 939) of the Niguarda "Ca' Granda" Hospital and was performed according to the Declaration of Helsinki.

Clinically identified seizure zone

Physicians identified the seizure zone (SZ) by visual inspection of SEEG traces. In focal epilepsy patients, seizures often originate from a well-defined seizure onset zone (SOZ), characterized by abnormal electrophysiological activity such as rapid low-voltage bursts, spike-wave discharges, and slow bursts with poly-spikes. Other regions within the pathological brain network, known as the seizure propagation zone (SPZ), do not initiate seizures but exhibit rhythmic changes shortly after seizure onset in the SOZ. In some cases, a brain region may be classified as both SOZ and SPZ, referred to as the seizure onset and propagation zone (SOPZ). For this study, we grouped SOZ, SPZ, and SOPZ under the broader term SZ. Any brain regions not identified as SZ were considered tentatively non-seizure zones (nSZ).

Raw feature extraction

Raw criticality and synchrony features were extracted following the methods described in previous studies[15,18], with a detailed description of the biomarkers available in the

Supplementary Methods. Criticality features were assessed for 20 narrow-band oscillations obtained with Morlet wavelets (m=5), ranging from 2 to 225 Hz with equal $\log_{10}$ spacing. They include critical exponent (DFA), bistability index (BiS), and the functional E/I balance index (fE/I). The DFA quantifies long-range temporal correlations (LRTCs) in a time series and is expected to show its global maximum inside an extended critical regime, *i.e.*, the Griffiths phase[14], where neuronal synchrony transit from near-zero to moderate synchrony (Fig. 2A). Within the Griffiths phase, the fE/I assessment characterizes three functional profiles—I-dominant, balanced, and E-dominant—based on correlation between time-resolved mean amplitudes and DFA assessments (profile 1–3, Fig. 2A). A brain region may show unimodal or bistable distribution in oscillation amplitudes (Fig. 2B–C, respectively), likely caused by an underlying positive feedback[15]. High bistability is a potent predictor of a catastrophic shift[21] towards supercritical, seizure-like events[18].

Phase synchrony was assessed using the phase-locking value (*PLV*) across 50 narrow-band frequencies, ranging from 2 to 450 Hz with equal $\log_{10}$ spacing. Each narrow-band *PLV* adjacency matrix characterized synchrony between all contact-pairs and was used to extract first- and second-order nodal features, characterizing the connectivity of each contact and its neighbors, respectively. First-order connectivity was estimated using eigenvector centrality and effective weight, while second-order connectivity was assessed using clustering coefficient and local efficiency.

The raw criticality features and synchrony were assessed using an in-house Python toolbox for a training set of 64 subjects, each with a 10-minute resting-SEEG recording (Fig. 1D). The first- and second-order nodal features of the *PLV* matrices were extracted using the Brain Connectivity Toolbox. For the test set, the same raw feature set was extracted from 7–9 hours of sleep-SEEG with a time-resolved approach, applying a 10-minute sliding window with a one-minute step size. The filtering and biomarker parameters were kept identical to those used for the training set. The resulting raw features for each subject form a three-way tensor ($X \in R^{k \times q \times t}$), representing k features, q contacts, and t time points (Fig. 1E).

Supervised classifiers

Based on observed spatial similarity in our previous studies, twenty normalized narrow-band criticality estimates were averaged into four frequency clusters as δ (2–4 Hz), θ − α (5.4–11 Hz), β (15–30 Hz), and γ1,2 (45–225 Hz). Similarly, fifty normalized narrow-band synchrony

features were collapsed into six frequency clusters as: δ − θ (2–5.4Hz), α (6.1–13 Hz), β (15–30 Hz), γ1 (40–96 Hz), γ2 (110–250 Hz), and γ3 (270–450Hz). To optimally separate SZ and nSZ contacts within subjects, normalization was done for each subject as: $\hat{x}_i = (x_i - \text{median}(X))./\max(X - \text{median}(X))$, where x_i represent a contact, X is a 1D vector of real numbers representing one narrow-band feature for all contacts for a given frequency. This dimensionality reduction resulted in 36 band-collapsed features to characterize each contact. For within-patient supervised classification of clinically identified SZ, we used leave-one-out validation (Fig. 2I), *i.e.*, a patient's contacts served as the test set and the remaining subjects formed the training set. To ensure robustness, we employed two classifiers: the Random Forest algorithm[33] and eXtreme Gradient Boosting (XGBoost)[34] from the scikit-learn toolbox[35]. Random Forest, previously used in our studies[15,18], is a machine learning method that leverages bootstrapped training data and combines decision tree simplicity with flexibility in handling new data. XGBoost, based on gradient boosting, sequentially refines decision trees by correcting previous errors, offering high speed, accuracy, and built-in regularization to prevent overfitting.

Spike density

Interictal epileptiform discharges (IEDs) are characterized by fast, high-amplitude transients lasting at least 200 ms[27], distinguishable from the background, and often spreading across multiple brain regions[30]. The IEDs were identified following the approach described in[18]. Briefly, for a 10-minute recording session of resting or sleep SEEG, we divided the broad-band signal from each SEEG contact into non-overlapping 0.5-second windows. A window was classified as 'spiky' if at least three consecutive samples exceeded seven times the standard deviation above the contact's mean amplitude. The spike density of a contact was then defined as the percentage of windows classified as spiky over the 10-minute session.

The EpiNet-saliency model

Design

An increase in seizure risk from baseline should be associated with multiple raw feature patterns such as strong synchrony and aberrant local criticality, most pronounced within and around the EpiNet as previously reported[15,18,29] (Fig. 1A). If the low-D epileptogenicity hypothesis holds, a brain region's pathological feature saliency over a time period could be

characterized by its trajectory in a low-D latent state space (Fig. 1B–C). The model was designed to be a lookup table using the two most predictive eigenfeature coefficients for the EpiNet as inputs, eliminating the need for retraining with new data and improving efficiency. Moreover, as seizure risk is known to fluctuate over hours[29,36], prolonged recordings are desirable to capture a full spectrum of the EpiNet-saliency.

Eigenfeature space of the resting-SEEG

Singular value decomposition (SVD) of the raw resting-state features is defined as:

$$X_{kq} = USV' \qquad (1)$$

where raw features $X_{kq} \in R^{k\times q}$ is a 2D array with each element represents k-th feature of q-th contact (k = 260 features, q = 7,183 contacts from 64 subjects); $U \in R^{k\times k}$ is a unitary matrix representing the full-rank eigenfeature space, with each of its column representing linear combination of raw-features (an example see Fig. 3C and Supplementary Fig. 1); $S \in R^{k\times q}$ is a rectangular diagonal matrix with singular values, and $V' \in R^{q\times q}$ is a unitary matrix, and both are not used.

Eigenfeature selection

The raw feature X_{kq} of the training data is projected into the full-rank eigenfeature space U:

$$\Phi = U'X_{kq} \qquad (2)$$

where the eigenfeature coefficients $\Phi \in R^{k\times q}$ represents the projection of raw features onto U. The effect size of difference between the SZ and nSZ contacts was assessed for each eigenfeature coefficient indexed by k, *i.e.*, $\Phi([SZ],k)$ vs $\Phi([nSZ],k)$ on the cohort level using Cohen's d. Only the ten coefficients that showed significant effect size compared to surrogate data were used to inform a rank-reduced $\widetilde{U} \in R^{r\times k}$ (r =10), representing an epileptogenicity-relevant sub-space of U that retains 10 of 260 of its original dimensions.

Train unsupervised classifiers

Since components of the EpiNet may overlap[3], algorithms allowing a contact to be assigned multiple clusters (soft-partition) are more suitable than hard-partition approaches used in our previous studies[15,18]. To examine whether epileptogenic neuronal dynamics can be differentiated in a rank-reduced eigenfeature space $\widetilde{U}$, we trained two unsupervised classifiers, Gaussian mixture models (GMM)[35] and Fuzzy C-means (FCM)[37], that support

soft-partition, allowing each contact to belong to different clusters with varying degrees of membership (M_i), with each $0 < M_i < 1$, and $sum(M_i) = 1$. We configured both classifiers to separate the EpiNet cluster and non-EpiNet cluster, hypothesizing that its members may include both SZ and nSZ regions (Fig. 1A). To ensure the robustness of the results, we tested both classifiers using an increasing number of coefficients (Φ), ranging from 2 to 10 with step size of two. In each test, an EpiNet membership and a non-EpiNet membership were assigned to each contact, which summed to one. The resulting EpiNet membership values across these tests were averaged for each contact, serving as a consensus EpiNet membership estimate ($\widehat{M}$) between two classifiers. A contact with $\widehat{M}$ approaching one is highly likely to be part of the EpiNet, while a value close to zero suggests it is unlikely.

Fitting and using the model

The (Φ_1–Φ_2) joint distribution for $<\widehat{M}>$ of the resting-SEEG, computed using 30 linear bins for both Φ_1 and Φ_2, forms a funnel-shaped surface but contains missing values (Fig. 3E). To make it a complete lookup table for all possible (Φ_1–Φ_2) combinations in new data, we fitted it as a smooth surface using MATLAB's Curve Fitting Toolbox with 'linear interpolant' method to approximate values between known data points and with 'linear extrapolation' for other missing data points. The resulting fitted surface represents the EpiNet-saliency assessment $\hat{\lambda} \in [0, 1]$ for a given contact in the (Φ_1–Φ_2) coordinate space, where $\hat{\lambda}$=1 indicates maximal saliency (Fig. 4A). To assess the assessment for a new contact, MATLAB function fitresult() is used by providing its Φ_1 and Φ_2 as inputs.

Test the model with sleep-SEEG

For each sleep-SEEG subject, time-resolved eigenfeature coefficient Φ_{qrt} was obtained by projecting the raw sleep features X_{kqt} into the rank-reduced eigenfeature space $\widetilde{U}_{rk}$ that is derived from the resting-SEEG (Eq. 2). The rank-1 and rank-2 coefficients (Φ_1, Φ_2) from Φ_{qrt} was then used as the input to the EpiNet-saliency model that returns an estimate $\hat{\lambda}(q, [\Phi_1, \Phi_2], t)$ for each contact q observed at time window t. Thus, given rank-1 and -2 coefficients [Φ_1, Φ_2] of a new contact q measured for time window t, the model returns an assessment $\hat{\lambda}(q, t)$. This can be done each contact across all the time windows. The average $\hat{\lambda}$ across contacts at time t characterizes a momentary global EpiNet-saliency $\hat{\Lambda}(t)$ for time window t.

Tensor component analyses

The canonical polyadic tensor decomposition[38] breaks down raw sleep feature (X_{kqt}), a three-way tensor, into a sum of rank-1 tensors, making it easier to analyze the hidden patterns in each of the three modes (Fig 5A left):

$$X_{kqt} = \sum_{r=1}^{R} \vec{\theta}_q^r \vec{\chi}_k^r \vec{\tau}_t^r \qquad (3)$$

where each term $\vec{\theta}_q^r \vec{\chi}_k^r \vec{\tau}_t^r$ in the sum corresponds to a *r*-th component's rank-1 approximation of the tensor (we set R = 20), with the contact vector $\vec{\theta}_q^r$ capturing a spatial pattern across q contacts showing k = 260 raw features captured by the feature vector $\vec{\chi}_k^r$, and the temporal profile vector $\vec{\tau}_t^r$ capturing a specific temporal pattern across all time points *t*. Summing over R such rank-1 components obtains a rank-R approximation of the raw sleep feature tensor X_{kqt} for one test subject.

Results

Feature overlap between SZ and nSZ reduces SZ-classification accuracy

Clinically identified SZ contacts typically exhibit bistable oscillation amplitudes in interictal period (Fig. 2D–E), along with larger LRTCs (Fig. 2F) and stronger functional inhibition (Fig. 2G). At the cohort level, the SZ shows a trend of increased bistability and inhibition in 15–225 Hz oscillations, slightly elevated LRTCs in 2–5 Hz and 30–225 Hz, and stronger phase synchrony in 2–300 Hz (Fig. 2H). To replicate our previous study on a smaller cohort[18], we trained wo supervised classifiers trained on band-collapsed raw features of the EZ. Both classifiers achieved similar accuracy in identifying the EZ (Fig. 2I), with a mean area under the receiver operating characteristic curve (AUC) of 0.74±0.14 (range 0.41–0.98), with two subjects performed below chance level. This variability in classification accuracy suggests substantial overlap between SZ and nSZ contacts, indicating the presence of nSZ contacts with SZ-like characteristics.

Ten eigenfeatures differentiate the seizure zone

To assess whether epileptogenic features are captured by a manageable number of latent variables for model training (Fig. 3A), we projected raw resting-SEEG features into the resting-SEEG eigenfeature space to obtain coefficients Φ (Eq. 1–2) and compared SZ and nSZ contacts across each Φ with Cohen's *d*. In cohort-pooled samples, over 50 coefficients were significant when compared to label-shuffled surrogate, with 10 remaining significant across individuals (Fig. 3B). The corresponding eigenfeature of the rank-1 Φ exhibited identical pattern of the SZ in our previous report[18]—characterized by strong bistability and inhibition in β–γ frequencies (Fig. 3B)—consistent with the high-seizure regime observed in computational models[15,18]. Notably, the rank-2 and 3 Φ exhibited increased γ-band excitation (Supplementary Fig. 1B), suggesting a significant contribution of excitation to the resting-SEEG feature.

The cohort-level joint probability distribution of the rank-1 and rank-2 coefficients forms a funnel-like surface, with the majority of contacts concentrated near its bottom (Fig. 3D). Across subjects, the SZ and nSZ were separated, with varying individual differences between SZ and nSZ (the length of the arrows in Fig. 3D). Since the coefficients were derived from only a 10-minute segment of interictal SEEG, it remains unclear whether this variability reflect a specific phase within a longer seizure cycle[36] at the time of recording or the mixing of nEZ between the EpiNet and non-EpiNet. Nonetheless, the observed smooth manifold suggests that it is feasible to use the coefficients to train a model to capture time-varying separability between the EpiNet and the non-EpiNet, and its associated seizure risk.

The EpiNet is identified with ten eigenfeature coefficients

The ten most significant coefficients that differentiated SZ and nSZ (Fig. 3B) were used to classify the EpiNet contacts. We simultaneously trained two classifiers to reach an agreement on how likely a contact belongs to the EpiNet, quantified as the consensus EpiNet-membership for each of the 7,183 contacts ($\widehat{M} \in \{0, 1\}$, with 0 and 1 indicating lowest and highest likelihood). Visualizing the mean membership $<\widehat{M}>$ across contacts in the (Φ_1–Φ_2) joint distribution (Fig. 3E) revealed a funnel-like surface that spatially separates the EpiNet contacts from the rest (Fig. 3E). Notably, individual SZ (arrowheads in Fig. 3D) predominantly fall within the EpiNet region (hot color in Fig. 3E), while the individual nSZ mostly locate (arrow-tails, Fig. 3D) falls in the non-EpiNet area (cold color in Fig. 3E).

To validate our previous findings[18,29], we investigated whether differences in $\widehat{M}$ estimates between SZ and nSZ account for variability in supervised SZ-classification accuracy (Fig. 2I) The within-subject difference in mean $\widehat{M}$ between SZ and nSZ correlates with the mean AUC of the two supervised classifiers for the SZ, with an effect size (r^2) of 0.5 (Fig. 3F). This suggests that when EpiNet nSZ and non-EpiNet nSZ regions are mixed (*i.e.*, EpiNet is more diffused into nSZ areas) or when the entire network is in a low seizure-risk phase (*i.e.*, a 10-minute window is insufficient to capture EpiNet features), the difference between SZ and nSZ in $\widehat{M}$ diminishes, leading to reduced supervised classification accuracy.

An EpiNet-saliency model constructed in a two-dimensional latent space

To determine whether EpiNet-membership estimates reflect epileptogenicity, we assessed correlation between $\widehat{M}$ estimates with mean spike density—a clinical biomarker for seizure risks (Fig. 3G). We found a moderate but significant correlation between $<\widehat{M}>$ and spike density (Spearman's r = 0.31, -log10(p) > 9.15, in total n = 371 non-zero elements from the (Φ_1–Φ_2) joint distributions in Fig. 3E&G), suggesting that $<\widehat{M}>$ indeed reflect seizure risk.

Furthermore, the $<\widehat{M}>$ estimates derived from the (Φ_1–Φ_2) joint distribution (Fig. 3E) — using only two of the ten coefficients—provided sufficient information for identifying EpiNet. The EpiNet-saliency model was then constructed by fitting the $<\widehat{M}>$ joint distribution as a smooth surface in the (Φ_1–Φ_2) coordinates representing saliency assessment $\hat{\lambda} \in \{0, 1\}$, where 0 and 1 indicating lowest and highest saliency, respectively, implying that samples resembling EpiNet exhibit higher seizure risk.

As a result, a parsimonious EpiNet-saliency model can be implemented as a lookup table, using the rank-1 and 2 coefficients from new data as inputs to obtain a saliency assessment, thereby reducing feature space to 1/130 of its original size and eliminating the need for re-training classifiers for new data.

The model is validated with sleep-SEEG data

To demonstrate the potential clinical value of our approach, we tested the model on three subjects from a separate cohort diagnosed with type 2 FCD. From subject *a* to *c*, clinical seizure risk increased, as reflected by a rising number of observed seizures during pre-

surgical monitoring and a greater number of contacts located in dysplastic cortex, confirmed by post-surgical histopathological analysis (Fig. 4B). Raw features were extracted for 10-minute sliding window with one-minute step size from 7–9 hours of sleep recorded over one night, enabling us to examine ultradian fluctuations in seizure risk as previously suggested[36]. After projecting the sleep raw features into the eigenfeature space (Fig. 1E), we compared raw features and coefficients Φ_1 and Φ_2 of resting- and sleep-SEEG. Their probability distributions largely overlapped, ruling out the possibility that any effects were driven by distributional shifts or outliers (Fig. 3C).

Ultradian fluctuations in Φ_1 and Φ_2 time series were observed in all three subjects (Fig. 4D). In the (Φ_1, Φ_2) latent space, trajectory of contacts located in FCD and non-FCD were separated (Fig. 4E), a trend that became more pronounced in time-averaged data (Fig. 4F), consistent with observations in the training set (Fig. 3D) and our hypothesis (Fig. 1C). Notably, abrupt changes in the coefficients coincided with sudden increases in time-resolved spike density (Fig. 4G), suggesting that the coefficients have captured the temporal fluctuations in seizure risk.

A potential functional dichotomy in interictal spikes

To investigate the correlation between EpiNet-saliency estimates and spike occurrences over time, we computed the mean spike density across contacts and applied the Hilbert transform to extract phase time series of the global spike density (middle, Fig. 4G). In all subjects, the contacts in FCD showed larger EpiNet-saliency assessments across all spike phases (top row, Fig. 4H), with effect sizes (bottom row, Fig. 4H) suggesting a trend of positive correlation with clinically identified seizure risk (Fig. 4B).

To better assess this trend, we grouped all samples into four spike phase bins, revealing an unexpected dichotomy in spike-related EpiNet-saliency modulation. As global spike density increased (0–90º), EpiNet-saliency in FCD contacts decreased in subjects *a* and *b* but increased in subject *c* who had the highest saliency (top row, Fig. 4I). When spike density decreased (90–180º), EpiNet-saliency in FCD contacts continued to decline in *a* and *b* but kept rising in *c*—suggesting that spikes in *a* and *b* may suppress seizure in the FCD, whereas in *c*, they appear to promote it.

Global EpiNet-saliency, defined as the average across all contacts, varied over time (Fig. 4J, top), which corroborate with fluctuations in classification accuracy based on contact-wise

saliency. Peak AUC of the classification reached 0.63, 0.85, and 0.94 in three test subjects (Fig. 4J, bottom). Both global and local EpiNet-saliency were consistent with clinical assessments of seizure risk, revealing a clear gradient of increasing risk from subject *a* to *c*. These results validate the model and offer new support for our low-dimensional epileptogenicity hypothesis at both local and global levels.

Validate mode prediction with tensor component analysis (TCA)

TCA was used to determine whether spike density and mode identified EpiNet-saliency are reflected in tensor components of individual raw sleep features. For each test subject, a total of R components (we used $R = 20$) were obtained by decomposition of raw sleep features, a three-way tensor (Fig. 5A), with each component providing a rank-1 reconstruction of the tensor, simultaneously capturing a distinct hidden pattern in the raw features $\vec{\chi}_k^r$ and its corresponding contact spatial map $\vec{\theta}_q^r$ and time course $\vec{\tau}_t^r$ (Eq. 3).

Pearson's correlation between two contacts (i, j) across contact vectors $\vec{\theta}_q^r$ (right, Fig. 5A) identifies contacts that remain similar in their raw feature patterns and temporal profiles across tensor components (TC). The TC similarity matrix (Fig. 5B) appears to have more detailed information about contact interactions than time-resolved EpiNet-saliency and spikes (Fig. 5B–D). The topology of these matrices was moderately correlated across subjects (Fig. 5E), suggesting that they capture shared information about the underlying brain networks.

To examine whether time-varying EpiNet-saliency are reflected in the TCs, we computed the Pearson's correlations between time vectors ($\vec{\tau}_t^r$) and both spike density (*e.g.*, Fig. 4G) and global EpiNet-saliency (Fig. 4K). In subject *a* and *b*, only one out of twenty TCs showed correlation between its $\vec{\tau}_t^r$ vector and global saliency but not with spikes. In *c*, one TC showed a correlation with both saliency and spikes (Fig. 5F–G). These results suggests that fluctuations in EpiNet-saliency have a sparse temporal representation in tensor space.

Next, we analyzed the generalizability and specificity of the raw feature patterns in the rank-1 EpiNet-relevant TC (highlighted in Fig. 5F). The rank-1 TC's feature vector $\vec{\chi}_k^r$ showed moderate Pearson's correlations between subjects, $r(a, b) = 0.23$, $r(a, c) = 0.21$, and $r(b, c) = 0.77$, indicating varying degrees of feature similarity across subjects. Notably, subject *b* and *c* are characterized by elevated bistability in 30–200 Hz and 10–200 Hz, consistent with previous findings[15,18], whereas *a*, who had the fewest seizures during pre-surgical study, showed elevated bistability centered at 10 Hz but not in the γ band (Fig. 5H). All test subjects

exhibited increased excitation, most prominently above 30 Hz, which contrasts with increased inhibition in the same band in the resting-SEEG (Fig. 3C).

Lastly, we examined differences between FCD and non-FCD contacts in the contact vector $\vec{\theta}_q^r$ of the rank-1 EpiNet-relevant TC, i.e., a larger $\vec{\theta}_q^r$ loading indicates more pronounced rank-1 EpiNet-relevant feature shown in (Fig. 5H). In subject *a* and *b*, the FCD contacts showed higher loading than non-FCD contacts (Fig. 5I) with large effect sizes (Cohen's d = -0.99 and -1.1, corresponding to 2.7 and 3.6 standard deviations (SD) above the mean of 10^4 surrogates, respectively). In subject *c*, however, the non-FCD contacts showed greater loading (Cohen's d = 1.3, 3.8 SD above the surrogate mean).

Discussion

Study recapitulation

We aim to address a long-standing challenge in understanding the systems-level complexity of epileptogenic mechanisms[3,39,40]. We asked whether the EpiNet can be characterized with invariant landmarks in a low-dimensional latent space that is reduced from hundreds of neuronal features—a hypothesis inspired by bifurcation models for local seizure dynamics[25,26]. To ensure the accessibility of the methods and results, we combined linear dimensionality reduction and white-box classifiers. We trained a model to assess EpiNet-saliency in a two-dimensional eigenfeature space and cross-domain tested the model on sleep-SEEG. The model not only identified clinically relevant EpiNet-saliency but also revealed unexpected, subject-specific relationships between the saliency and spikes. Independent tensor component analysis further validated the model, reinforcing its rigor.

EpiNet-saliency reflects systems-level seizure risk in state space, as its estimates in both training and test sets correlate with interictal spikes. However, since only interictal data were used for training, the exact location of seizure bifurcation—onset, offset, and refractory state—within the latent space is not demarcated. Therefore, EpiNet-saliency in the latent space characterizes a degree of epileptogenic proneness and should not be interpreted as a measure of distance to bifurcation onset nor as a prediction of seizure imminence.

Novelty: a framework for unified biomarkers

While mechanistic understanding of the EZ has advanced significantly over the last seven decades[39], presurgical EZ-localization remains a complex process relying on multidisciplinary expertise and extensive clinical infrastructures[3,9,41]. The sensitivity and specificity of any single biomarker is nonetheless limited by various conceptual and practical factors[8,9,27,40,42–44], and no existing framework is capable of comprehensively utilizing all relevant biomarkers.

To fill this gap, we recently proposed shifting the focus from a discrete EZ to a broader epileptogenic network (EpiNet), combining multiple biomarkers with machine-learning to achieve more comprehensive localization[18,29]. The current study aimed to resolve the high-D challenge inherent in our earlier approach and provided initial proof of concept for a scalable framework to decipher systems-level complexity of the EpiNet, bridging novel biomarkers and data science approaches with clinical needs.

EpiNet characterized in a latent space

The model takes two eigenfeatures as input, reducing dimensionality to 0.77% of the original features—without compromising individual sensitivity due to band-wise feature averaging in previous studies[15,18]. This not only resolves the challenge in model training but simplifies interpretation. The rank-1 eigenfeature unfolds as elevated inhibition, bistability, and LRTCs in 30–225 Hz oscillations, indicative of aberrant criticality with a catastrophic shift—a pattern in line with findings from both theoretical and empirical studies[15,18,45]. The EpiNet-saliency in new data can be assessed by projecting the raw features into the eigenfeature space and retrieving the saliency score from the trained model, eliminating the need for retraining. This approach significantly reduces computational overhead, supports analysis of large clinical datasets, and may potentially be adapted for online seizure forecasting.

EpiNet characterized on a minute-level timescale

Seizure prediction is most meaningful on a minute-level timescale, as it not only allows sufficient time for intervention[46,47], improves computational efficiency[29], but also grounded in physiological foundations. Bifurcation models[25,26] suggest a slow *permittivity* variable that controls an ensemble's operating distance to seizure bifurcation. Numerous mechanisms—such as synaptic, metabolic, electrophysiological, and anatomical/functional changes—may

synergize and contribute to temporal fluctuations in the permittivity. This suggests that the seizure dynamics should not be attributed to a few isolated mechanisms, but rather treated as a latent variable[25], as considered here.

In the sleep-SEEG, global EpiNet-saliency fluctuated on a multi-minute scale and correlated with spike density and rank-1 tensor component. At the local level, SZ and nSZ exhibited time-varying contrast in EpiNet-saliency, reflecting ultradian evolution in seizure risks[36]. Similar fluctuations are likely present in the resting-SEEG[36]. As a result, the SZ-vs-nSZ contrast during 10-minute resting-SEEG could have varied substantially across subjects—a variability leads to poor classification accuracy, particularly for subjects recorded during a low seizure risk phase when the contrast is weak. This individual variability, however, is desired in model training as it would generalize to the gradient in new data.

Individual variability in EpiNet features

The finding that many non-SZ contacts resemble SZ features suggests that even physiologically normal regions can operate in a pathological regime as previously suggeseted[18]. Clinically, this reinforces the notion that some regions may facilitate seizure without being able to independently generate seizures. Such regions may be suboptimal targets for resection but suitable candidates for neuromodulation[9,47,48].

All three test subjects showed considerable fluctuations in EpiNet-saliency during sleep, while their bistability profiles—derived from the rank-1 EpiNet-relevant tensor component—differed significantly, despite sharing the same FCD histopathology. One patient exhibited broad α–γ band bistability and experienced the most frequent seizures, while another showed only α-band bistability and had only one observed seizure.

Collectively, these findings suggest that although functional biomarkers offer greater granularity than structural pathology alone[3,9], the timing of SEEG recording is crucial. If data are only sampled during a low-risk phase, the EpiNet extent may be underestimated, and its feature pattern may also generalize poorly. This dynamic property of EpiNet-saliency is both a strength and a limitation—the temporal sampling bias warrants future investigation.

Inhibition and excitation in the latent space

Recent computational modelling has shown that in a critical-like regime with high bistability, increasing neuronal coupling is associated with local dynamics to first exhibit inhibition, then

excitation, and eventually supercritical, seizure-like hypersynchrony[18]. The SZ in both resting- and sleep-SEEG showed elevated bistability, implying a regime shift toward supercritical regime[15,18,21].

In the rank-1 eigenfeature of resting-SEEG, increased 30–225 Hz inhibition was observed, whereas increased 30–225 Hz excitation characterized both the sleep-SEEG and lower-rank eigenfeatures of the resting-SEEG. This suggests that some resting-SEEG subjects could have been closer to seizure onset than others. Given that FCD is frequently associated with sleep-related epilepsy[32], it is possible that the test subjects were indeed closer to seizure onset during sleep than most of the resting-SEEG subjects—likely operating on the overexcited, supercritical side of the critical regime as our modelling study has suggested[14]. Despite this potential between-cohort difference, the model cross-domain identifies the FCD contacts, suggesting that variation in a specific raw feature set had little impact on overall prediction.

A possible functional dichotomy in spikes

Spike density was correlated with EpiNet-saliency in both resting- and sleep-SEEG. Time-resolved analyses revealed subject-specific correlations between spike density and EpiNet-saliency during sleep: in the subject who had most frequent seizures, saliency increased following a rise in spikes, suggesting that the spikes are likely excitatory and thus promote seizure; in the other two, following a rise in spikes, saliency decreased, suggesting a possible protective role of the spikes.

Although based on only three cases, these results provide independent support—through the lens of systems-level neuroscience—for the hypothesis of a functional dichotomy of spikes[8,49–53] and the possibility of distinct spike-generating mechanisms[54]. This may help explain why spikes often appear across widespread regions outside the EZ, diminishing their specificity despite being an established clinical biomarker[55,56]. Another preliminary study using resting-magnetoencephalography suggests that, rather than a binary distinction, the spatiotemporal organization of spikes may follow a continuum reflecting slow fluctuations in E/I balance[57].

Limitations and future efforts

This innovative approach facilitates the inclusion of additional biomarkers and, importantly, may provide an answer to why established clinical biomarkers often lose specificity[24].

However, it remains an open question whether histopathological substrates (*e.g.*, hippocampal sclerosis vs FCD), comorbidities, or brain states are encoded in separate latent variables or interact with those relevant to the EpiNet. Such interactions may exist in the sleep-SEEG, as ultradian fluctuations in seizure risk during sleep is likely driven by the NREM–REM cycle, where epileptiform activity is typically suppressed during REM sleep and promoted during N2 stage of NREM[36,58], likely over large-scale connectivity[45]. Comorbid disorders are highly prevalent among epilepsy patients[59]. However, due to limited access to clinical information, we here were unable to investigate comorbidity.

Our model was trained on interictal resting-state data. As such, EpiNet-saliency should be interpreted as the likelihood that a region is part of the EpiNet based what the model learned from systems-level features—rather than as a direct measure of proximity to seizure bifurcation, as in models[25] and SEEG studies[27] based on local dynamics. Seizure onset can be classified using electrophysiological signatures generated by four known bifurcations[25,27,28]. Therefore, it is feasible to empirically estimate the distance to bifurcation with the biomarkers employed here and in recent studies[23,45,60]—but at a second-level resolution, rather than minute-level resolution considered here.

Despite its gold-standard signal quality[41], SEEG is costly, invasive, limited in accessibility, making it unsuitable for repeated measures or large-scale screening. SEEG implants are guided by clinical hypotheses, which may lead to under-sampling in complex cases[61]. As a next step, we will test this approach for whole-brain, non-invasive mapping with source-reconstructed MEG or scalp EEG[62,63].

Conclusion

This work advances a methodological breakthrough for hypothesis-free characterizing the EpiNet. It sets a clear line of sight from this innovative approach through a powerful framework that synergizes information across diverse biomarkers—aimed at advancing collaborative standardization in presurgical EZ mapping, mechanistic studies, and beyond[64].

Data availability

Compliance with Italian governing laws and Ethical Committee regulations prohibits the sharing of raw SEEG data and patient information. However, interim data and final results

that support the findings of this study can be obtained from the corresponding authors upon reasonable request.

Funding

This study has been supported by a Sigrid Jusélius Foundation Fellowship awarded to SHW (210527). LN and GA were supported by NEXTGENERATIONEU (NGEU) and by the Ministry of University and Research (MUR), National Recovery and Resilience Plan (NRRP), project MNESYS (PE0000006)—A Multiscale integrated approach to the study of the nervous system in health and disease (DN. 1553 11.10.2022). This project was also funded by: Academy of Finland grant (SA 253130 and 296304) awarded to JMP and Sigrid Jusélius Foundation grant awarded to SP and JMP. MM was supported by the DARLING Project (Projet-ANR-19-CE48-0002) obtained by PC from Agence Nationale de la Recherche, France. SHW was partially supported by the DARLING Project.

Competing interests

All authors report no competing interests.

References

1. Devinsky O, Vezzani A, O'Brien TJ, et al. Epilepsy. *Nat Rev Dis Prim*. 2018;4(May). doi:10.1038/nrdp.2018.24
2. Luders H, Engel J, Munari C. *Surgical Treatment of the Epilepsies.* Raven Press; 1993.
3. Zijlmans M, Zweiphenning W, van Klink N. Changing concepts in presurgical assessment for epilepsy surgery. *Nat Rev Neurol*. 2019;15(10):594-606. doi:10.1038/s41582-019-0224-y
4. Stacey W, Kramer M, Gunnarsdottir K, et al. Emerging roles of network analysis for epilepsy. *Epilepsy Res*. 2020;159(December 2019):106255. doi:10.1016/j.eplepsyres.2019.106255
5. Khambhati AN, Davis KA, Oommen BS, et al. Dynamic Network Drivers of Seizure Generation, Propagation and Termination in Human Neocortical Epilepsy. *PLoS Comput Biol*. 2015;11(12):1-19. doi:10.1371/journal.pcbi.1004608
6. van Lanen RHGJ, Colon AJ, Wiggins CJ, et al. Ultra-high field magnetic resonance imaging in human epilepsy: A systematic review. *NeuroImage Clin*. 2021;30(February):102602. doi:10.1016/j.nicl.2021.102602
7. Jacobs J, Zijlmans M, Zelmann R, et al. High-frequency electroencephalographic oscillations correlate with outcome of epilepsy surgery. *Ann Neurol*. 2010;67(2):209-220. doi:10.1002/ana.21847
8. Guth TA, Kunz L, Brandt A, et al. Interictal spikes with and without high-frequency oscillation have different single-neuron correlates. *Brain*. 2021;144(10):3078-3088. doi:10.1093/brain/awab288
9. Miller KJ, Fine AL. Decision-making in stereotactic epilepsy surgery. *Epilepsia*. Published online November 1, 2022. doi:10.1111/epi.17381
10. Astner-Rohracher A, Zimmermann G, Avigdor T, et al. Development and Validation of the 5-SENSE Score to Predict Focality of the Seizure-Onset Zone as Assessed by Stereoelectroencephalography.

JAMA Neurol. 2022;79(1):70-79. doi:10.1001/jamaneurol.2021.4405
11. Cardinale F, Rizzi M, Vignati E, et al. Stereoelectroencephalography: Retrospective analysis of 742 procedures in a single centre. *Brain*. 2019;142(9):2688-2704. doi:10.1093/brain/awz196
12. Bulacio JC, Bena J, Suwanpakdee P, et al. Determinants of seizure outcome after resective surgery following stereoelectroencephalography. *J Neurosurg*. 2022;136(6):1638-1646. doi:10.3171/2021.6.JNS204413
13. Auno S, Lauronen L, Wilenius J, Peltola M, Vanhatalo S, Palva JM. Detrended fluctuation analysis in the presurgical evaluation of parietal lobe epilepsy patients. *Clin Neurophysiol*. 2021;132(7):1515-1525. doi:10.1016/j.clinph.2021.03.041
14. Fuscà M, Siebenhühner F, Wang SH, et al. Brain criticality predicts individual synchronization levels in humans. *Nat Commun*. Published online 2023:2022.11.24.517800. doi:doi.org/10.1038/s41467-023-40056-9
15. Wang SH, Siebenhühner F, Arnulfo G, et al. Critical-like brain dynamics in a continuum from second-to first-order phase transition. *J Neurosci*. 2023;43(45):7642-7656. doi:10.1523/JNEUROSCI.1889-22.2023
16. Beggs JM. The criticality hypothesis: How local cortical networks might optimize information processing. *Philos Trans R Soc A Math Phys Eng Sci*. 2008;366(1864):329-343. doi:10.1098/rsta.2007.2092
17. Monto S, Vanhatalo S, Holmes MD, Palva JM. Epileptogenic neocortical networks are revealed by abnormal temporal dynamics in seizure-free subdural EEG. *Cereb Cortex*. 2007;17(6):1386-1393. doi:10.1093/cercor/bhl049
18. Wang SH, Arnulfo G, Nobili L, et al. Neuronal Synchrony and Critical Bistability: Mechanistic Biomarkers for Localizing the Epileptogenic Network. *Epilepsia*. Published online 2024. doi:doi.org/10.1101/2023.05.21.541570
19. van van Hugte EJH, Schubert D, Nadif Kasri N. Excitatory/inhibitory balance in epilepsies and neurodevelopmental disorders: Depolarizing γ-aminobutyric acid as a common mechanism. *Epilepsia*. 2023;64(8):1975-1990. doi:10.1111/epi.17651
20. Lepeu G, van Maren E, Slabeva K, et al. The critical dynamics of hippocampal seizures. *Nat Commun*. 2024;accepted(July 2023). doi:10.1038/s41467-024-50504-9
21. Thom R. *Structural Stability and Morphogenesis*. 1st Ed. CRC Press; 1972. https://www.taylorfrancis.com/books/9780429493027
22. Siebenhühner F, Wang SH, Arnulfo G, et al. Genuine cross-frequency coupling networks in human resting-state electrophysiological recordings. Poeppel D, ed. *PLOS Biol*. 2020;18(5):e3000685. doi:10.1371/journal.pbio.3000685
23. Myrov V, Siebenhühner F, Juvonen JJ, Arnulfo G, Palva S, Palva JM. Rhythmicity of neuronal oscillations delineates their cortical and spectral architecture. *Commun Biol*. 2024;7(1):1-18. doi:10.1038/s42003-024-06083-y
24. Zweiphenning W, van MA, C Klink NE, et al. *Intraoperative Electrocorticography Using High-Frequency Oscillations or Spikes to Tailor Epilepsy Surgery in the Netherlands (the HFO Trial): A Randomised, Single-Blind, Adaptive Non-Inferiority Trial*. Vol 21.; 2022. www.thelancet.com/neurology
25. Jirsa VK, Stacey WC, Quilichini PP, Ivanov AI, Bernard C. On the nature of seizure dynamics. *Brain*. Published online 2014. doi:10.1093/brain/awu133
26. Saggio ML, Spiegler A, Bernard C, Jirsa VK. Fast–Slow Bursters in the Unfolding of a High Codimension Singularity and the Ultra-slow Transitions of Classes. *J Math Neurosci*. 2017;7(1):1-47. doi:10.1186/s13408-017-0050-8
27. Saggio ML, Crisp D, Scott JM, et al. A taxonomy of seizure dynamotypes. *Elife*. 2020;9:1-56. doi:10.7554/eLife.55632
28. Izhikevich EM. Neural excitability, spiking and bursting. *Int J Bifurcat Chaos*. 2000;10(6):1171-1266. doi:10.1142/S0218127400000840
29. Wang S, Marzulli M, Arnulfo G, et al. Machine learning models trained in a low-dimensional latent space for epileptogenic zone (EZ) localization. In: *EUSIPCO*. ; 2024.
30. Arnulfo G, Wang SH, Myrov V, et al. Long-range phase synchronization of high-frequency oscillations in human cortex. *Nat Commun*. 2020;11(1). doi:10.1038/s41467-020-18975-8
31. Arnulfo G, Hirvonen J, Nobili L, Palva S, Palva JM. Phase and amplitude correlations in resting-state activity in human stereotactical EEG recordings. *Neuroimage*. 2015;(112):114-127.
32. Gibbs SA, Proserpio P, Francione S, et al. Clinical features of sleep—related hypermotor epilepsy in

relation to the seizure—onset zone : A review of 135 surgically treated cases. *Epilepsia*. 2019;(April):707-717. doi:10.1111/epi.14690
33. Breiman L. Random Forests. In: *Machine Learning*. Vol 45. Kluwer Academic Publishers; 2001:5-32.
34. Chen T, Guestrin C. XGBoost: A scalable tree boosting system. *Proc ACM SIGKDD Int Conf Knowl Discov Data Min*. 2016;13-17-Augu:785-794. doi:10.1145/2939672.2939785
35. Pedregosa F, Varoquaux G, Gramfort A, Michel V, Thirion B. Scikit-learn: Machine Learning in Python. *J Mach Learn Res*. 2011;12:2825-2830. doi:10.1289/EHP4713
36. Karoly PJ, Rao VR, Gregg NM, et al. Cycles in epilepsy. *Nat Rev Neurol*. 2021;17(5):267-284. doi:10.1038/s41582-021-00464-1
37. Warner J, The scikit-fuzzy development team. scikit-fuzzy: Fuzzy Logic Toolbox for Python. Published 2018. github.com/scikit-fuzzy/scikit-fuzzy
38. Kolda TG, Bader BW. Tensor decompositions and applications. *SIAM Rev*. 2009;51(3):455-500. doi:10.1137/07070111X
39. Lara Jehi. The Epileptogenic Zone: Concept and Definition. *Epilepsy Curr*. 2018;18(1):12-16.
40. Fisher RS, Scharfman HE, DeCurtis M. How Can We Identify Ictal and Interictal Abnormal Activity? *Adv Exp Med Biol*. Published online 2014:3-23. doi:10.1007/978-94-017-8914-1_1
41. Frauscher B, Mansilla D, Abdallah C, et al. Learn how to interpret and use intracranial EEG findings. *Epileptic Disord*. 2024;26(1):1-59. doi:10.1002/epd2.20190
42. Perucca P, Gotman J. Delineating the epileptogenic zone: spikes versus oscillations. *Lancet Neurol*. 2022;21(11):949-951. doi:10.1016/S1474-4422(22)00396-9
43. Gliske S V., Irwin ZT, Chestek C, et al. Variability in the location of high frequency oscillations during prolonged intracranial EEG recordings. *Nat Commun*. Published online 2018. doi:10.1038/s41467-018-04549-2
44. Fisher RS, Cross JH, French JA, et al. Operational classification of seizure types by the International League Against Epilepsy: Position Paper of the ILAE Commission for Classification and Terminology. *Epilepsia*. 2017;58(4):522-530. doi:10.1111/epi.13670
45. Burlando G, Belforte C, Siebenhühner F, et al. Sleep-Modulated Cross-Frequency Coupling Between δ Phase and β-γ Bistability: A System-Level Modulation of Epileptic Activity. *bioRxiv*. 2025;(125):1-30. https://www.biorxiv.org/content/10.1101/2025.03.25.642592v1
46. Qi Z, Liu H, Jin F, et al. A wearable repetitive transcranial magnetic stimulation device. *Nat Commun*. 2025;(September 2024):1-14. doi:10.1038/s41467-025-58095-9
47. Nair DR, Laxer KD, Weber PB, Murro AM, Park YD. Nine-year prospective e ffi cacy and safety of brain- responsive neurostimulation for focal epilepsy. *Neurology*. 2020;0(95(9)). doi:10.1212/WNL.0000000000010154
48. Rao VR, Rolston JD. Unearthing the mechanisms of responsive neurostimulation for epilepsy. *Commun Med*. 2023;3(1):1-6. doi:10.1038/s43856-023-00401-x
49. Shi W, Shaw D, Walsh KG, et al. Spike ripples localize the epileptogenic zone best: an international intracranial study. *Brain*. 2024;147(7):2496-2506. doi:10.1093/brain/awae037
50. Rasmussen T. Characteristics of a Pure Culture of Frontal Lobe Epilepsy. *Epilepsia*. 1983;24(4):482-493. doi:10.1111/j.1528-1157.1983.tb04919.x
51. Serafini R. Similarities and differences between the interictal epileptiform discharges of green-spikes and red-spikes zones of human neocortex. *Clin Neurophysiol*. 2019;130(3):396-405. doi:10.1016/j.clinph.2018.12.011
52. Schaft E V., Sun D, van 't Klooster MA, et al. Spatial and temporal properties of intra-operatively recorded spikes and high frequency oscillations in focal cortical dysplasia. *Clin Neurophysiol*. 2024;162:210-218. doi:10.1016/j.clinph.2024.03.038
53. Karoly PJ, Freestone DR, Boston R, et al. Interictal spikes and epileptic seizures: Their relationship and underlying rhythmicity. *Brain*. 2016;139(4):1066-1078. doi:10.1093/brain/aww019
54. Curtis M De, Avanzini G. Interictal spikes in focal epileptogenesis. *Prog Neurobiol*. 2001;63:541-567.
55. Ung H, Cazares C, Nanivadekar A, et al. Interictal epileptiform activity outside the seizure onset zone impacts cognition. *Brain*. Published online 2017. doi:10.1093/awx178
56. Smith EH, Merricks EM, Davis T, et al. Human interictal epileptiform discharges are bidirectional traveling waves echoing ictal discharges. *Elife*. 2022;11(73541):1-20.
57. Ferrari P, Wang SH, Moreau T, et al. Non-invasive MEG localization of Excitatory and Inhibitory Spikes. In: *American Epilepsy Society*. ; 2024.
58. Nobili L, Frauscher B, Eriksson S, et al. Sleep and epilepsy: A snapshot of knowledge and future research lines. *J Sleep Res*. 2022;31(4):1-11. doi:10.1111/jsr.13622

59. Keezer MR, Sisodiya SM, Sander JW. Comorbidities of epilepsy: Current concepts and future perspectives. *Lancet Neurol*. 2016;15(1):106-115. doi:10.1016/S1474-4422(15)00225-2
60. Dumeur M, Wang SH, Palva JM, Ciuciu P. Multifractality in critical neural field dynamics. Published online 2023:1-6. http://arxiv.org/abs/2312.03219
61. Jaber K, Avigdor T, Mansilla D, et al. A spatial perturbation framework to validate implantation of the epileptogenic zone. *Nat Commun*. 2024;15(1):1-17. doi:10.1038/s41467-024-49470-z
62. Bagic A, Funke ME, Ebersole J. Magnetoencephalography (MEG)/Magnetic Source Imaging (MSI) in Noninvasive Presurgical Evaluation of Patients With Medically Intractable Localization-related Epilepsy. *J Clin Neurophysiol*. 2009;26(4):290-293.
63. Maldjian JA, Lee R, Jordan J, et al. ACR White Paper on Magnetoencephalography and Magnetic Source Imaging: A Report from the ACR Commission on Neuroradiology. *Am J Neuroradiol*. 2022;43(12):E46-E53. doi:10.3174/ajnr.A7714
64. McKee HR, Vidaurre J, Clarke D, et al. It's About Time! Timing in Epilepsy Evaluation and Treatment. *Epilepsy Curr*. Published online 2024. doi:10.1177/15357597241238072

Figure legends

Figure 1

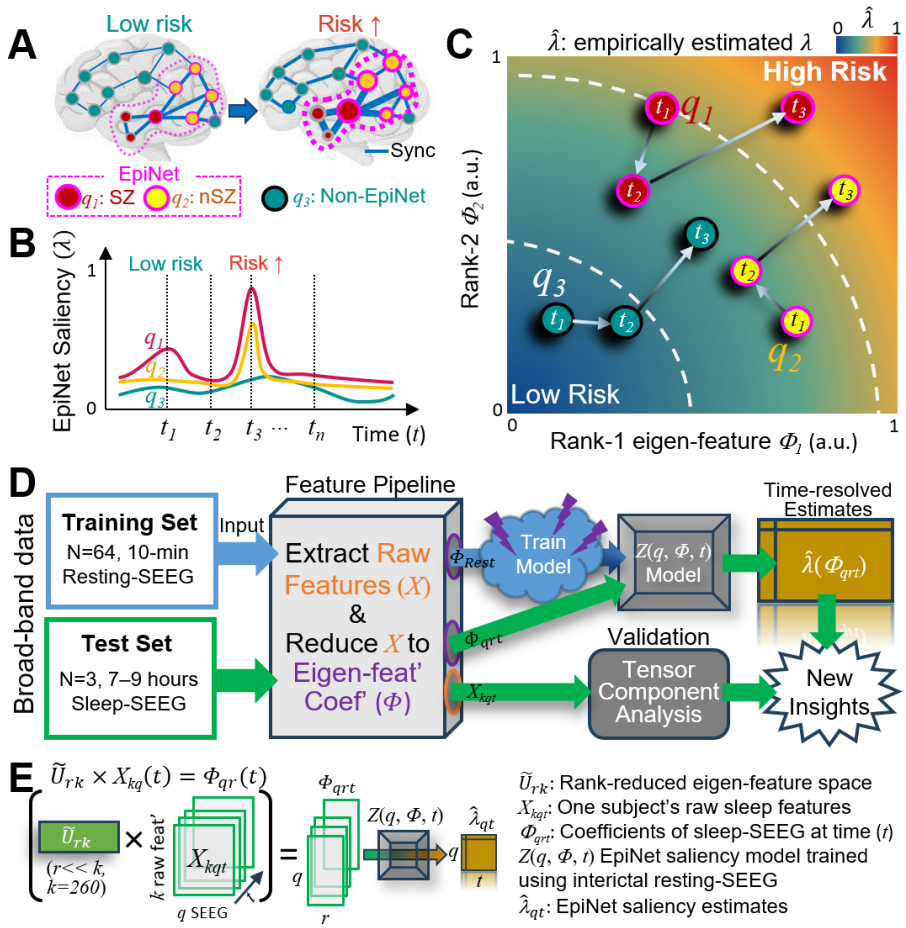

Study design. (A–C) The hypothesis. **(A)** An increased seizure risk is associated with aberrant local (nodes) criticality and strong synchrony (edges) within and around the epileptogenic network (EpiNet). **(B)** As seizure risk increases, the EpiNet, including its constituent seizure zone (SZ) and non-SZ (nEZ), exhibits more salient pathological features (larger λ) than other regions (q_3). The saliency of the EpiNet fluctuates over time (t). **(C)** High-dimensional interictal raw brain dynamics features of a training dataset are projected into a low-dimensional eigenfeature space, allowing classifiers to be trained to assess individual regions' EpiNet-saliency ($\hat{\lambda}$). **(D)** The analysis pipeline. **(E)** Test the low-D EpiNet-saliency model with sleep-SEEG. Matrix multiplication (×): project one subject's raw sleep features $X_{kq}(t)$ into the eigenfeature space $\tilde{U}_{rk}$ derived from resting-SEEG. The resulting coefficients Φ_{qrt} is used as input for the model. q: number of SEEG contacts; r: reduced rank<< raw feature number $k = 260$; t: number of observation windows with 10-minute resolution.

Figure 2

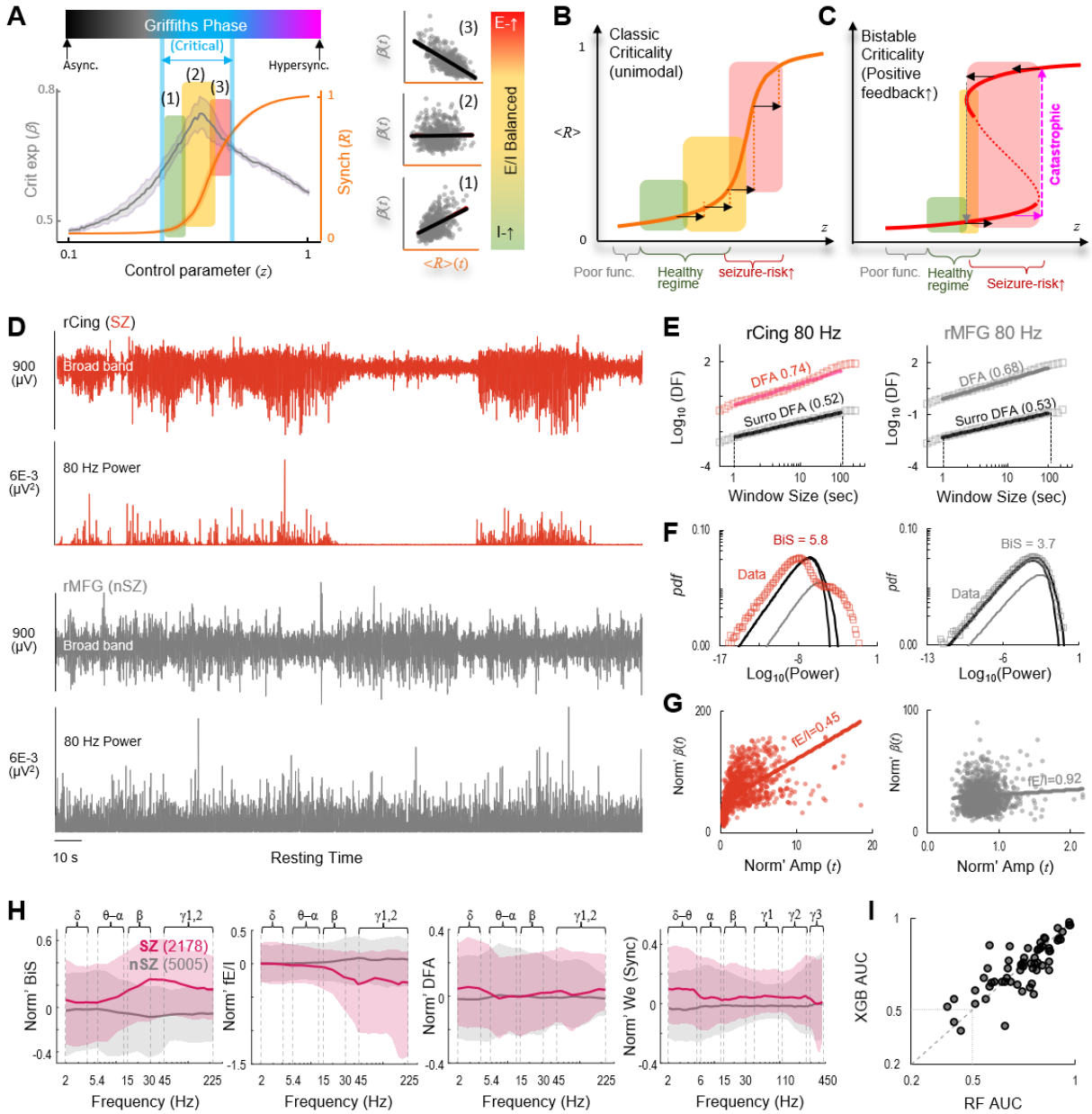

Feature overlap between seizure zone (SZ) and non-SZ (nSZ) introduces variability in accuracy of supervised SZ-classification. (A–C) Theoretical motivation for the biomarkers. **(A)** Three excitation/inhibition (E/I) profiles inside an extended critical regime (Griffiths phase) based on time-resolved analysis. In insets, Markers indicate temporal samples. The neuronal dynamical regime of **(B)** classic criticality and **(C)** bistable criticality. **(D)** Broad-band and narrow-band time series of resting-SEEG from a SZ and a nearby nSZ contact. rCing: right cingulate; rMFG: right middle frontal gyrus. **(E–G)** The fitting of criticality metrics for the time series from **(D)**. **(E)** Computation of critical exponents of long-range temporal correlations (DFA), **(F)** bistability index (BiS), and **(G)** functional E/I estimate (fE/I). **(H)** Within-subject normalized narrow-band biomarkers. We: effective weight of phase synchrony. Shaded areas: 25% and 75%-tile. **(I)** Supervised SZ-classification accuracy. AUC: area under receiver operating characteristics curve. Markers: subjects; Two classifiers, RF (Random Forest) and XGB (XGBoost), were trained with band-collapsed features derived from (H).

Figure 3

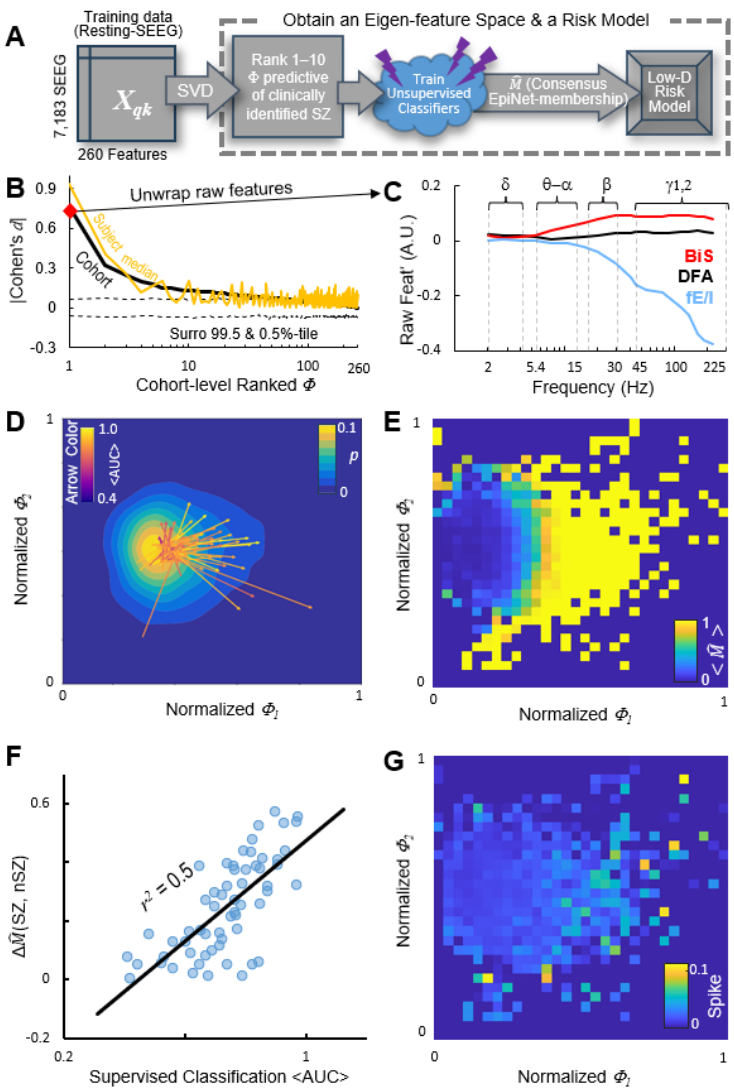

Obtain eigenfeature coefficients to train a model to assess EpiNet-saliency. (A) Pipeline. **(B)** Cohort pooled (black) and median of subject level (N=64, yellow) differences across coefficients between the SZ and nSZ, ordered by population Cohen's *d*. Dashed lines: surrogate confidence intervals. **(C)** Normalized features of the rank-1 eigenfeature. **(D)** Cohort joint distribution is a 2D representation of a funnel-like manifold. Arrows: subjects; arrowhead: SZ; arrow-tail: nSZ. **(E)** Mean EpiNet-membership ($\widehat{M}$) across the contacts from the (Φ_1–Φ_2) joint distribution. **(F)** Correlation between supervised SZ-classification accuracy (from Fig 2I) and the within-subject difference in $\widehat{M}$ between SZ and nSZ. **(G)** Joint distribution of mean contact spikes.

Figure 4

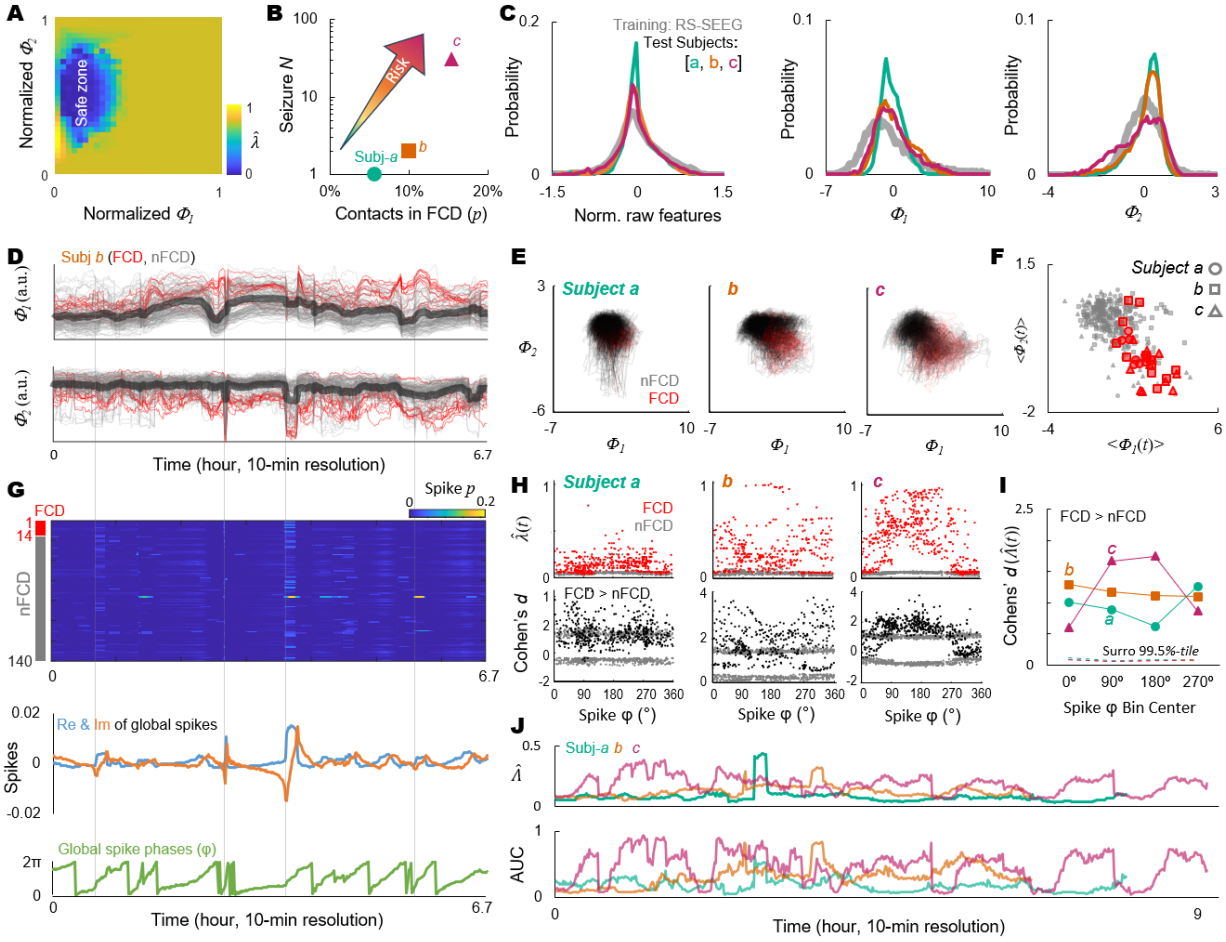

Cross-domain validate the model. (A) The EpiNet-saliency model visualized as a 2-dimensional lookup table. **(B)** Total number of seizure events observed during pre-surgical monitoring as a function of contacts inside dysplastic cortices (FCD). **(C–F)** Properties of Φ_1 and Φ_2. **(C)** Probability distribution of normalized raw features, Φ_1, and Φ_2 of the training and test subjects, with all features of all contacts pooled. **(D)** One subject's individual contacts and mean (thick) Φ_1 and Φ_2 over time with temporal resolution of 10-minute. **(E)** All contacts' trajectory overlaid. **(F)** Time-averaged Φ_1 and Φ_2; subjects' contacts are identified by marker shape defined in **(B)**. **(G)** Spikes observed from the same subject's recording whose (Φ_1, Φ_2) are shown in (D). Top: contact spike density; middle: real (Re) and imaginary (Im) part of mean spike density across contacts; bottom: phases of mean spike density. **(H)** Top: distributions of EpiNet-saliency as a function of spike phases; bottom: distributions of effect sizes of differences between FCD and nFCD in EpiNet-saliency as a function of spike phases, gray markers represent surrogate observation. **(I)** Effect sizes in four spike phase bins. Dashed line: confidence interval observed from 10^3 label-shuffled surrogates. **(J)** Top: time-resolved global EpiNet-saliency (mean across contacts); bottom: area under receiver-operating characteristic curve.

Figure 5

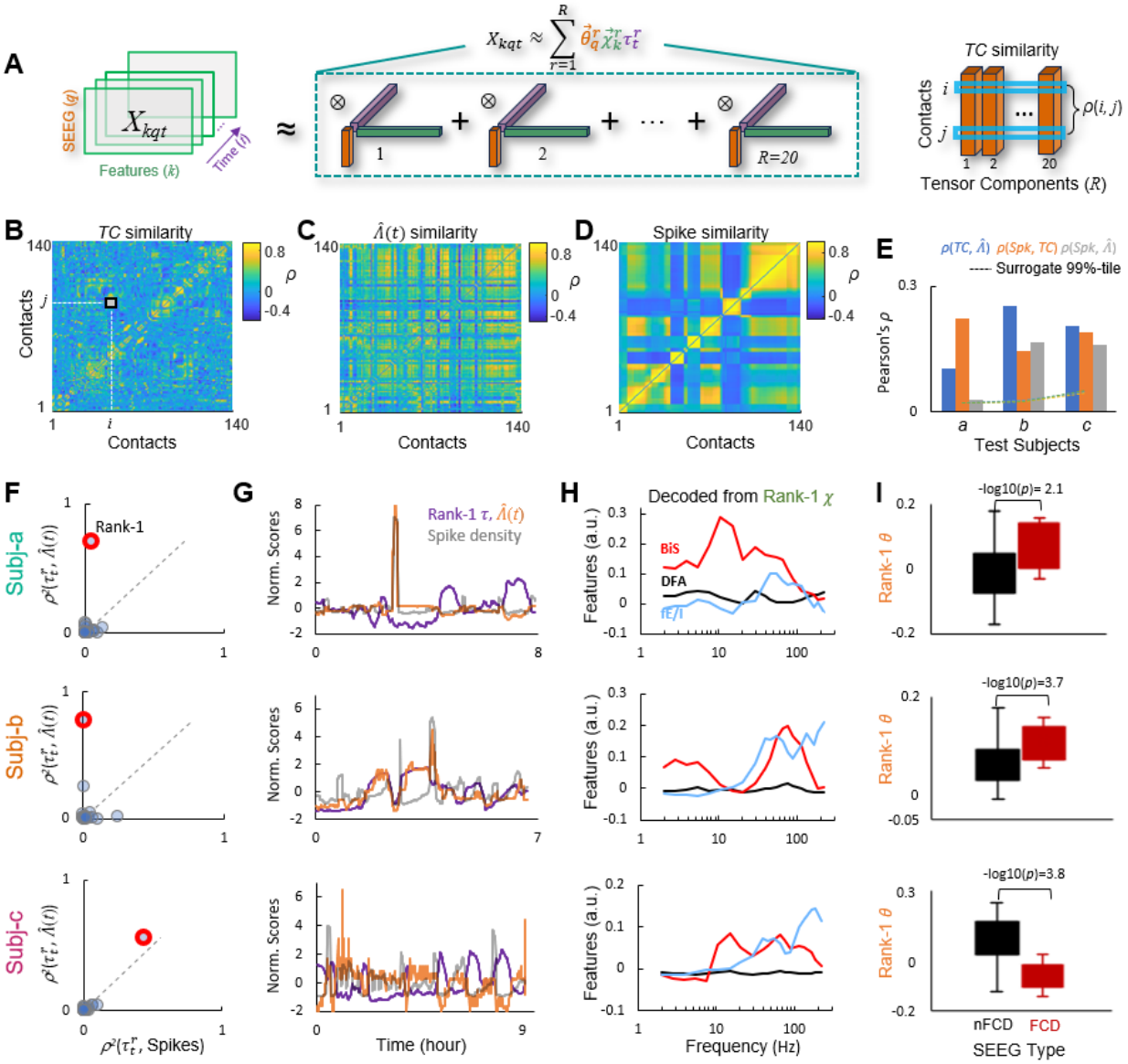

Tensor component analysis (TCA) identifies components that correlate with EpiNet-saliency and spikes while revealing individual-specific details. (A) Left: canonical (polyadic) tensor decomposition of one subject's raw sleep features. Right: inter-contact similarity is the correlation between their tensor components (TC), with subject b's TC similarity as an example shown in **(B)**. **(B–D)** An example of one subject's inter-contact similarity by **(B)** TC, **(C)** EpiNet-saliency $\hat{\lambda}(t)$, and **(D)** spike density. **(E)** Cross correlations between the three contact similarity matrices for the three test subjects. Dashed: confidence intervals of 1,000 surrogates. **(F–I)** TCA for the three test subjects. **(F)** Effect size of Spearman's correlation (ρ^2) between time-loading τ_t^r (purple vectors in **A**) and the global EpiNet-saliency ($\hat{\lambda}$) as a function of correlations between the τ_t^r and spikes. Markers: 20 TCs. **(G)** Time series rank-1 τ_t^r highlighted in **(F)**, global EpiNet-saliency, and spikes**.** Normalization: $(x - mean(x))/std(x)$. **(H)** Visualization of raw feature of the rank-1 feature-vector χ (green vector in **A**). BiS: bistability index; DFA: critical exponent; fE/I: functional E/I index. **(I)** Differences (unpaired t-test) between contacts inside focal cortical dysplasia (FCD) and non-FCD in the rank-1 contact-vector θ (purple vector in **A**).